AD-A069 955 NAVAL POSTGRADUATE SCHOOL MONTEREY CA F/G 15/1
THE USE OF TEMPERATURE AND COLOR IN SATELLITE DETECTION OF OCEA--ETC(U)
FEB 79 E D TRAGANZA
UNCLASSIFIED NPS-68-79-008 NL

1 OF 1
AD
A069955

END
DATE FILMED
7-79
DDC

NPS-68-79-008

NAVAL POSTGRADUATE SCHOOL

Monterey, California

THE USE OF TEMPERATURE AND COLOR IN SATELLITE DETECTION OF OCEAN FRONTS AND EDDIES FOR ASW APPLICATIONS

A Summary of Selected Literature Condensed and Edited

by

Eugene D. Traganza

February, 1979

Technical Report Period	July to September 1978

Approved for public release; distribution unlimited.

Prepared for: Commander, Naval Ocean Systems Center
San Diego, California 92152

NAVAL POSTGRADUATE SCHOOL
Monterey, California

Rear Admiral Tyler F. Dedman
Superintendent

Jack R. Borsting
Provost

The work reported herein was supported by the Naval Ocean Systems Center, San Diego, California 92152.

This report was prepared by:

Eugene D. Traganza
Associate Professor of Oceanography

Reviewed by

Warren W. Denner, Principal Investigator
Associate Professor of Oceanography

Approved by

D. F. Leipper, Chairman
Department of Oceanography

W. M. Tolles
Dean of Research

Unclassified

SECURITY CLASSIFICATION OF THIS PAGE (When Data Entered)

REPORT DOCUMENTATION PAGE		READ INSTRUCTIONS BEFORE COMPLETING FORM
(14) 1. REPORT NUMBER NPS-68-79-008	2. GOVT ACCESSION NO.	3. RECIPIENT'S CATALOG NUMBER
(6) 4. TITLE (and Subtitle) The Use of Temperature and Color in Satellite Detection of Ocean Fronts and Eddies for ASW Applications. A Summary of Selected Literature Condensed & Edited		5. TYPE OF REPORT & PERIOD COVERED 6. PERFORMING ORG. REPORT NUMBER
(10) 7. AUTHOR(s) Eugene D. (and) Traganza		8. CONTRACT OR GRANT NUMBER(s)
9. PERFORMING ORGANIZATION NAME AND ADDRESS Naval Postgraduate School Code 63Tg Monterey, California 93940 251 450		10. PROGRAM ELEMENT, PROJECT, TASK AREA & WORK UNIT NUMBERS N6600178WR00120
11. CONTROLLING OFFICE NAME AND ADDRESS Commanding Officer Naval Ocean Systems Center - Attn: Code 531 San Diego, CA 92152		(11) 12. REPORT DATE February 1979 13. NUMBER OF PAGES 58
(9) 14. MONITORING AGENCY NAME & ADDRESS(if different from Controlling Office) Technical rept. Jul-Sep 78,		15. SECURITY CLASS. (of this report) Unclassified 15a. DECLASSIFICATION/DOWNGRADING SCHEDULE
16. DISTRIBUTION STATEMENT (of this Report) Approved for public release; distribution unlimited. (12) 60 p.		
17. DISTRIBUTION STATEMENT (of the abstract entered in Block 20, if different from Report)		
18. SUPPLEMENTARY NOTES		
19. KEY WORDS (Continue on reverse side if necessary and identify by block number) Satellites, Ocean Fronts, Temperature, Color, ASW		
20. ABSTRACT (Continue on reverse side if necessary and identify by block number) The purpose of this report is to briefly update the state of the art of detection of ocean fronts and eddies by satellite sensed sea surface temperature and to consider oceanographic color characteristics which may be used to detect their presence when the sea surface temperature pattern is absent. 252 450 slk		

DD FORM 1 JAN 73 1473 (Page 1) EDITION OF 1 NOV 65 IS OBSOLETE S/N 0102-014-6601

1

Unclassified

SECURITY CLASSIFICATION OF THIS PAGE (When Data Entered)

79 06 04 032

TABLE OF CONTENTS

LIST OF FIGURES

LIST OF TABLES

LIST OF PLATES

I. INTRODUCTION (Effects of ocean fronts and eddies on ASW)

Ocean fronts and eddies (OFAE) have been observed in every ocean and major sea as thermal "discontinuities" associated with current boundaries or regions of upwelling (Figure 1). The affect of oceanographic characteristics of fronts and eddies on underwater sound propagation is important in pro- and anti-submarine warfare (PSW and ASW). Fronts and eddies can extend over hundreds to thousands of miles and frequently occur in areas of strategic importance where submarines could use them to avoid detection from surveillance and tactical sonar systems. In addition biological activity frequently increases in the vicinity of these features and can result in high ambient noise and volume reverberation levels. The acoustic characteristics of OFAE and their potential application by Fleet ASW forces are well documented in the summary report "Effects of Ocean Fronts and Eddies on ASW in the North Atlantic" by Crocker and Spikes (1977). These reviewers bring out the point that, if fronts and eddies can be charted on a real-time basis, the Navy can directly apply the knowledge gained in frontal acoustics to ASW surveillance and tactics. Currently ocean fronts and eddies are remotely sensed from satellites by infrared radiation derived sea surface temperature (SST). There are some problems. For example, cold core eddies in the Gulf Stream region lose their surface temperature characteristics in the first three months of their estimated two year life time. Although strong horizontal thermal gradients persist below the surface, the satellite images show no anomalous surface thermal patterns. Cloud cover can alter the IR sea surface temperature information and sometimes completely obliterate it. Forty to 50 percent of the earth is obscured by clouds on any given day. In one study of the Gulf Stream region significant features could be located on 14 out of 30 days in the spring

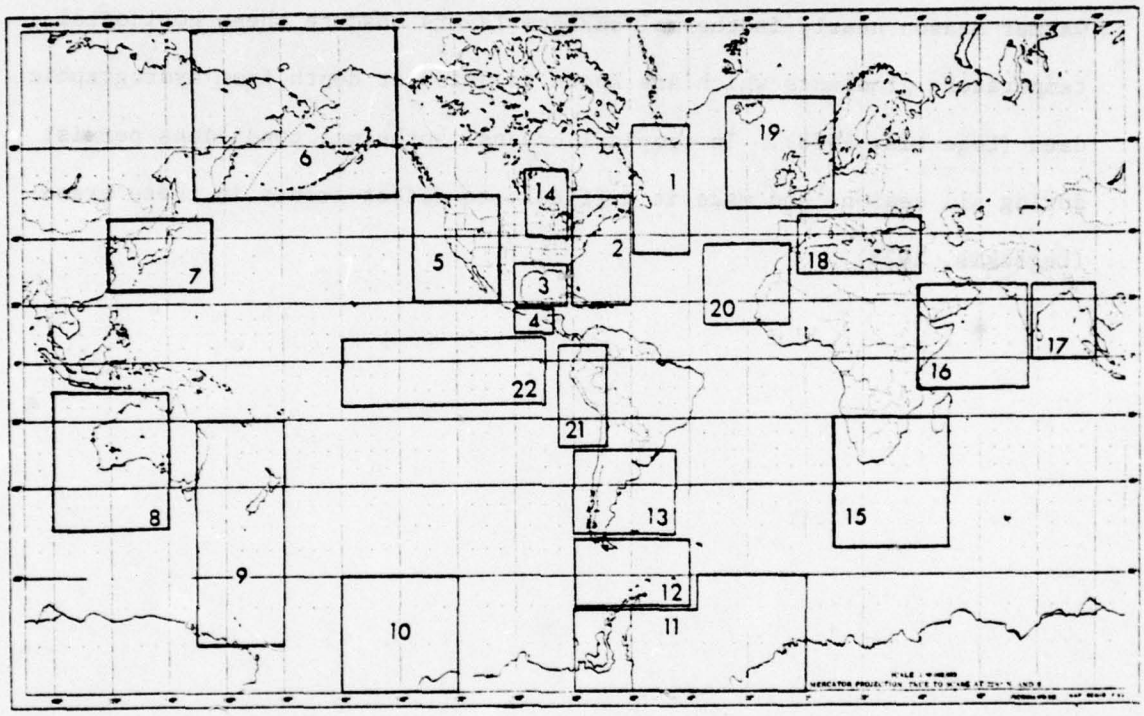

Figure 1. The areas of the world in which sea surface temperature fronts have been observed in satellite thermal infrared images are outlined from 1 to 22 on the map of the world (from Legeckis, 1978).

and only 6 of 30 in winter with periods when the sea surface was not visible for two weeks at a time (Crocker and Spikes, 1977). Detection of fronts is limited according to season for a different reason (Legeckis, 1978). In winter months the ocean's upper layers tend to be well mixed so that horizontal temperature gradients such as those associated with deeper currents are also recognizable at the sea surface (Legeckis, 1978). During the warmer season nearly isothermal surface layers obscure these horizontal temperature gradients which are known to exist at depth from hydrographic data (Legeckis, 1978). In tropical oceans isothermal conditions persist during all seasons and make it difficult to detect fronts in these areas (Legeckis, 1978).

II. OBJECTIVE

The purpose of this report is to briefly update the state of the art of detection of ocean fronts and eddies by satellite sensed sea surface temperature and to consider oceanographic color characteristics which may be used to detect the presence of OFAE from satellite images when the SST pattern is not present.

III. DETECTION OF OCEAN FRONTS AND EDDIES BY SATELLITE SENSED SEA SURFACE TEMPERATURE

A. POLAR AND GEOSTATIONARY SATELLITES
(A condensation from Legeckis, 1978)

"It was during the early days of weather monitoring by orbiting satellites that it was postulated that the IR measurements could also be used to detect sea surface temperatures (SST) in cloud-free ocean areas. However, the IR images of the sea surface were of marginal quality for the interpretation of SST fronts. As a result, most oceanographers either ignored the satellite-derived results or were not convinced that satellite observations could be integrated usefully with classical oceanographic observations. The recent improvement of infrared scanners on the polar and geostationary environmental satellites operated by the National Oceanic and Atmospheric Administration (NOAA) has enabled the detection of many sea surface temperature fronts associated with ocean currents and upwelling."

"In 1972 a very high resolution radiometer (VHRR) was introduced in the polar-orbiting satellites operated by NOAA. The main improvement was the increase of spatial resolution (IFOV, ~ 1 km) and the decrease of signal noise (NEΔT, 0.5° -3°C). As a result of observations made by the VHRR, SST fronts associated with currents and upwelling could be detected. For example, upwelling off the coast of western Africa, Gulf Stream instabilities, upwelling off Mexico, eddies off the California coast, the position of the Polar front in the Drake Passage, and the Agulhas Current system were described."

"Another significant development in the detection of ocean fronts from satellites occurred in 1974 with the launching of a Geostationary Operational Environmental Satellite (GOES). By 1975, two of these satellites

were located above the equator at 75° and 135° longitude. Although the spatial resolution of this satellite is coarse (IFOV, 8 km), the low signal noise (NEΔT, 0.3°C) allows SST fronts to be detected and monitored. The advantage of the GOES is that observations are made every 30 minutes, thus allowing cloud motions to be resolved. Because SST fronts remain nearly stationary over a period of a day, it is often possible to use time sequences of IR images to observe the fronts as the clouds move in relation to them."

i. Infrared Data

"The first VHRR data from the NOAA polar-orbiting satellites became available in 1972. Four of these satellites (NOAA 2, 3, 4, and 5, operated sequentially) provided data until 1978. The visible data are recorded in the wavelength range from 0.6 to 0.7 μm and the IR from 10.5 to 12.5 μm with a spatial resolution (IFOV) of 1 km and an IR temperature sensitivity of 0.5°C. Large areas of the ocean surrounding the North American continent are monitored by the VHRR twice daily by receiving stations located at Wallops Island, Virginia; Redwood City, California; and Fairbanks, Alaska. In addition, it is possible to obtain VHRR data in any area of the world (approximately a 3000-km square) by first recording the data on the satellite and then retransmitting them upon passing a receiving station. This type of coverage is limited by the on-board satellite recording capability."

"A second important source of data is provided by the GOES system with the visible and infrared spin-scan radiometer (VISSR). The data are available in the visible wavelengths from 0.55 to 0.75 μm and in the IR from 10.5 to 12.6 μm. The spatial resolution for the visible data is variable (IFOV, 1-8 km), whereas that for the IR is fixed at 8 km. The IR

temperature sensitivity is approximately 0.5°C. The GOES satellite rotates in the same direction as the earth so that it remains essentially stationary above the equator. The data, useful for ocean fronts, extends to 50° of latitude and longitude around the subpoint of the satellite. The United States presently operates two of these satellites with subpoints located at longitudes 75° and 135°W. By 1978 there will be Japanese and European geostationary satellites in operation. The U.S.S.R. is expected to provide a similar satellite somewhat later. This system of five geostationary satellites will allow continuous observations of the entire earth equatorward of 60° latitude."

"In 1978 the NOAA satellite system will be replaced by the next generation of NOAA polar orbiters, called TIROS N. This system will have the capability for global (4-km resolution) and regional (1-km resolution) observations of the oceans four times each day. Because of several improvements in the new radiometer and in the data transmission procedures, it is expected that the electronic noise will be reduced (NEΔT, 0.2°C). This improvement should allow the detection of ocean fronts at both the 1- and the 4-km spatial resolution range and will greatly increase the quantity of useful data. Because the polar-orbiting satellite transmits data continuously, it is possible for anyone to receive the data, provided one has the proper equipment."

"When the improved data became available from the VHRR and the VISSR instruments, the Environmental Data Service, an agency of NOAA, established a facility in Washington, D. C., to archive and distribute the satellite data. Presently, all visible and IR images are archived as photographic negatives. In addition, digital data are also saved in limited quantities. In most applications of satellite data for the study of ocean

fronts it is more useful to have the digital data rather than the archived photographic images. The reason for this is that the archived photographs are usually not processed specifically for the optimum detection of ocean fronts. The digital data provide the flexibility to present the data for specific applications in both a qualitative and a quantitative format. Some ocean-related data processing is done at the National Environmental Satellite Service (NESS), Satellite Data Services Branch, Washington, D. C. 20233."

ii. Noise

"To appreciate the effects of noise in the IR images, one must consider how these images are produced. The satellite data are collected by repeated scanning of the earth's surface. Adjacent scans are displayed as a two-dimensional array of data to create a photographic image. The variations of the electronic signal, referred to as the net equivalent change in temperature (NEΔT), produce random or coherent two-dimensional noise patterns superimposed on the SST signal radiated from the earth. When the noise patterns are of comparable magnitude to the SST gradients associated with fronts, it becomes difficult to distinguish them from each other."

iii. Cloud Cover

"Clouds often obscure the surface of the ocean. Since IR radiation is absorbed by water vapor, clouds are a severe limitation in making observations of SST fronts. The clearest views of SST fronts are associated with the passage of atmospheric cold fronts which are followed by large areas of relatively cold, dry air. Cloud formations can sometimes be used to locate the SST fronts."

iv. Atmospheric Attenuations

"Thermal IR radiation is absorbed by water vapor, aerosols, carbon dioxide, and ozone. Therefore depending on atmospheric conditions, the ocean temperature can appear to be 1° - 10°C lower at the satellite IR sensor than at the sea surface. The temperature corrections are estimated to range from 1° to 10°C for water vapor, 0.1° to 1°C for aerosols, and 0.1°C for the CO_2 and O_3. Although atmospheric absorption reduces the absolute values of sea surface temperatures as recorded by the satellite, the relative distribution of ocean temperatures can be measured within the limitation of noise and the spatial variations of the atmospheric corrections. To correct for the effects of atmospheric absorption, one must have access to the distribution of the moisture field in the atmosphere. Methods of resolving this problem have been proposed."

v. Image Enhancement

"The original purpose of introducing satellite IR sensors was to allow meteorologists to observe clouds during the night as well as during the day. To appreciate why special data processing is sometimes required to make full use of the IR data for the detection of ocean fronts, it is necessary to consider how the data are processed for most meteorological applications."

"The satellite infrared detectors have a temperature response from approximately -90°C to +60°C. The infrared data in this temperature range are normally displayed on gray tone photographic film to produce images of clouds, land, and water. The colder parts of the scene, such as clouds, are assigned lighter shades of gray, whereas the warmer scenes, such as land and water, appear as darker shades of gray. Because the range of sea surface temperature extends from about 0° to 40°C, it is advantageous

to assign the available shades of gray within this narrower temperature range, thus allowing the ocean SST fronts to be distinguished more clearly. This method of data processing is called image enhancement. The lack of properly enhanced satellite data can prevent the detection of SST fronts in the standard meteorological photographic products."

vi. Geometric Corrections

"Satellite images are geometrically distorted because of the method of data acquisition and the curvature and rotation of the earth. An important consideration in the study of ocean fronts is the availability of satellite data which are presented in the same geometric perspective to allow a sequence of images to be compared. The problem is more apparent with polar-orbiting satellites because successive views of the same area on the earth are made from different angles. The geostationary satellite data, while also geometrically distorted, are obtained from nearly the same position relative to the satellite subpoint so that successive images have nearly the same perspective. Thus geostationary satellite images can be compared directly without geometric corrections."

"The degree to which polar-orbiting satellite data must be corrected geometrically depends on the accuracy required. The accurate mapping of data requires either precise satellite navigation information or landmarks which can be identified on the image."

vii. Ocean Fronts Detected by the VHRR Infrared Scanners

"The VHRR scanners have been used to survey ocean fronts on a worldwide basis. Usually, the visible images are used to find cloud-free areas of the ocean, and the infrared images are used to detect the SST fronts. When visible images are not available, it is usually possible to distinguish SST fronts from cloud patterns by pattern recognition and by

the relative spatial stationarity of SST fronts over a period of several days. The areas of the world in which the VHRR data have been obtained are shown in Figure 1. Areas 1-6 have been monitored continuously twice per day since 1972. All other areas have been monitored intermittently."

viii. Color

The advent of satellite sensing of ocean color differences may allow detection of ocean fronts when nearly isothermal surface temperatures prevent their recognition with infrared sensors (Legeckis, 1978).

IV. SATELLITES, SENSORS, PRODUCTS AND APPLICATIONS

A. NOAA-5 (Launched September, 1976)

The following for the most part is a condensation from Kalinowski et al (1977) beginning with a brief discussion of the satellite and its sensors followed by a summary of relevant products and applications. "The last in the current series of polar-orbiting satellites, designated NOAA 5, has been fully operational since September, 1976. As with other satellites in the series, NOAA 5 is near-circular, 102° inclination orbit (see Figure 2 for inclination effects) and completes approximately 12.4 1500-kilometer altitude orbits per day, permitting two looks per day (night and day) at each point on the earth. Its sensor complement includes a Solar Proton Monitor, a Vertical Temperature Profile Radiometer (VTPR), a Scanning Radiometer (SR) and a Very High Resolution Radiometer (VHRR). The SR has two channels, visible and thermal infrared (10.5 - 12.5 μm), with about 4.2- and 8.0-km resolutions, respectively. Similar channels in the VHRR both have 0.9 km resolution. The VTPR is an eight-channel atmospheric sounder with six channels in the 15 μm CO_2 band, one water vapor and one thermal infrared window channel."

i. Scanning Radiometer (SR) and Vertical Temperature Profile Radiometer (VTPR)

a. Global Sea Surface Temperature (Daily Observations)

"The main quantitative oceanographic product now available is the Global Operational Sea Surface Temperature Computation (GOSSTCOMP) (Figure 3). Observations are produced from target arrays of SR infrared data, evaluated for cloud contamination, corrected for atmospheric attenuation, and then quality controlled. VTPR data are used in these procedures

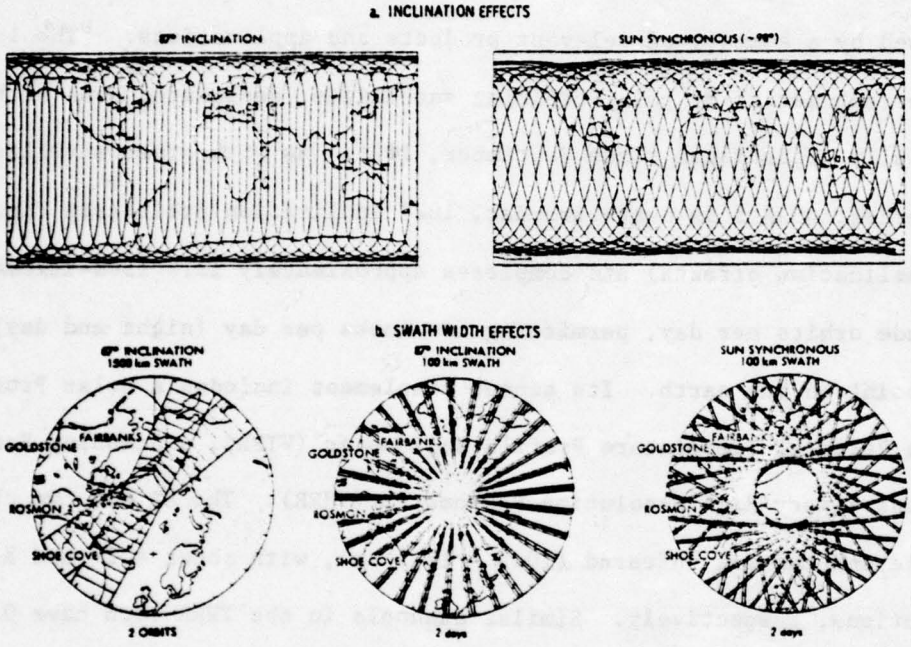

Figure 2. A comparison of near polar (87° inclination) and sun synchronous orbit earth-tracks (from Nagler, 1977).

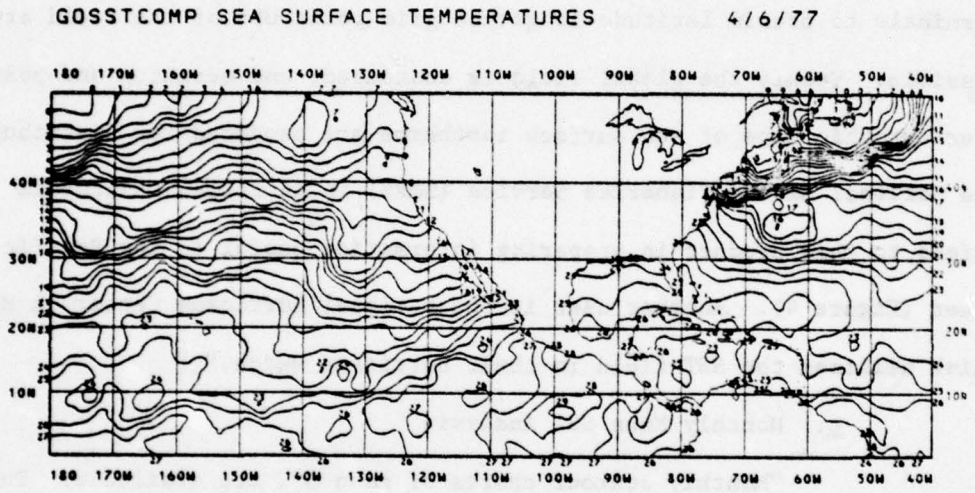

Figure 3. Global Operational Sea Surface Temperature Computation (GOSSTCOMP) for April 6, 1977, derived daily from the NOAA satellite series (NOAA-5 for this analysis) using the Scanning Radiometer (SR). Temperature retrievals are statistically averaged over approximately a 100-km square area (from Sherman, 1977).

when available; otherwise, empirically derived corrections are applied."

"Each day a tape of SST observations is supplied to the U. S. Navy for use in its Fleet Numerical Weather Center SST field analysis. With access to the NOAA computer lists of the current days observations could be obtained via remote terminal at sea."

b. Global SST Fields (Weekly Composites)

"Each day the Objective Analysis Technique (OAT) merges new SST observations into the global polar-stereographic SST field. Remote terminals to obtain latitude-longitude grid pointouts of the field are possible. Weekly the global field is contoured, and mercator and polar-stereographic maps of sea surface isotherms are produced for distribution. The national Marine Fisheries Service (NMFS) in La Jolla, California refers to this product in preparing information useful to the Pacific tuna fleet (Figure 4). Another user is the National Hurricane Center in Miami, which utilizes the SST field in their hurricane watch."

c. Monthly Mean SST Analysis

"Monthly contour charts of mean SST are available. This product should be valuable as an anomaly and climatic change analysis tool."

ii. Very High Resolution Radiometer (VHRR); Visible and Infrared Spin Scan Radiometer (VISSR)

"Oceanographic products employing the high resolution data of the VHRR and VISSR are primarily qualitative in nature and most often in the form of or derived from "enhanced" imagery. These products have their greatest utility in the depiction of relative temperature differences, although absolute calibrations using external sources of data is possible."

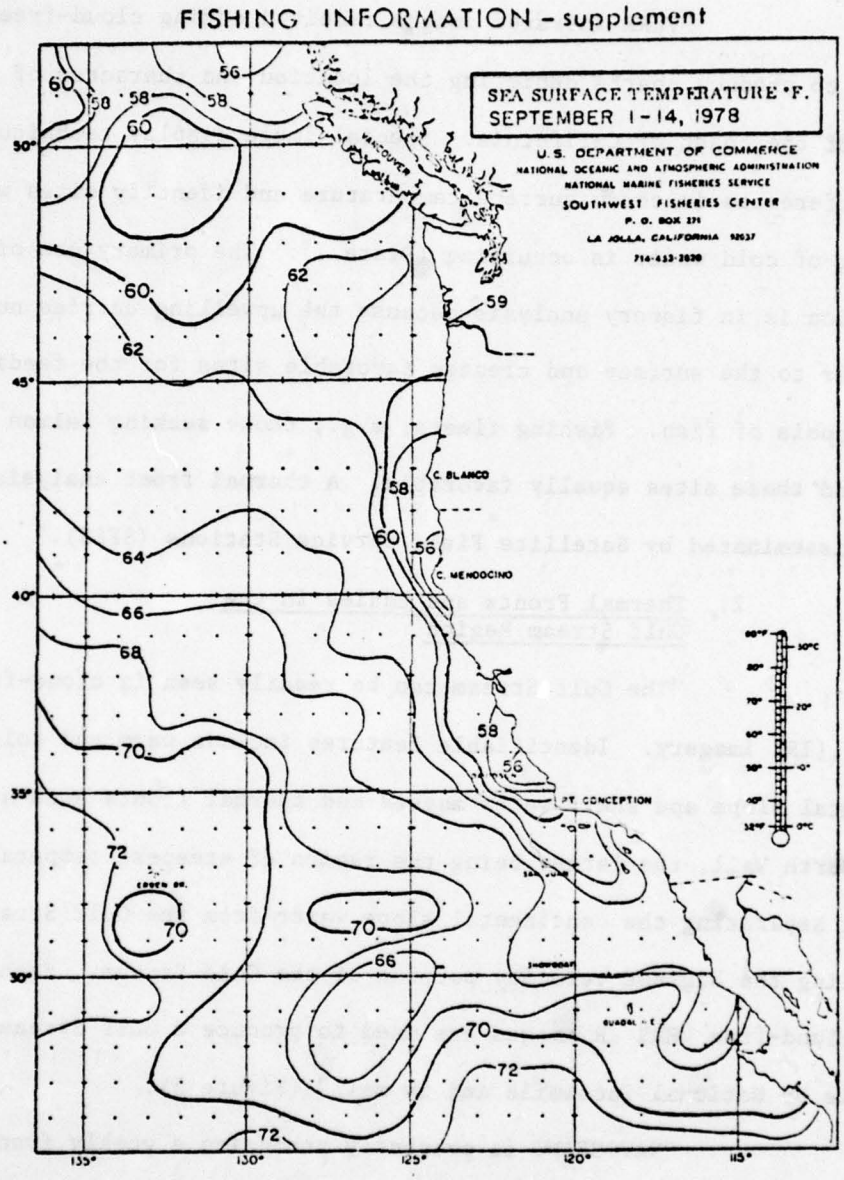

Figure 4. Sea surface temperature, °F, September 1-14, 1978 (from the Fishing Information Supplement U.S. Department of Commerce NOAA, NMFS, Southwest Fisheries Center, La Jolla, California).

a. Ocean Thermal Front Analysis

1. Thermal Fronts and Eddies in the California Current and Coastal Region

"VHRR infrared images received during cloud-free periods are used to produce charts depicting the location and character of thermal fronts off the coast of California. Special image display techniques enhance differences in ocean surface temperature and identify sites where upwelling of cold water is occurring (Plate I). The primary use of this information is in fishery analysis because the upwelling carries nutrient-rich water to the surface and creates favorable sites for the feeding of large schools of fish. Fishing fleets; e.g., those seeking salmon and tuna, often find these sites equally favorable. A thermal front analysis (Figure 4a) is disseminated by Satellite Field Service Stations (SFSS)."

2. Thermal Fronts and Eddies in the Gulf Stream Region

"The Gulf Stream can be readily seen in cloud-free VHRR infrared (IR) imagery. Identifiable features include warm and cold eddies, continental slope and shelf water masses and thermal fronts such as the Gulf Stream North Wall, the latter being the region of steepest temperature gradient separating the continental slope water from the Gulf Stream and paralleling the highest velocity portion of the Gulf Stream. Each week the latest cloud-free VHRR IR images are used to produce a Gulf Stream Analysis available by National Facsimile and by mail" (Figure 5).

"NAVOCEANO is presently producing a weekly frontal chart of the western North Atlantic Ocean based primarily on NOAA-5 satellite infrared (IR) imagery. Copies of the chart are telecopied to Fleet Numerical Weather Central, Monterey, Fleet Weather Central (FWC) Norfolk, and can be provided to other commands for operational planning" (Crocker and Spikes, 1977).

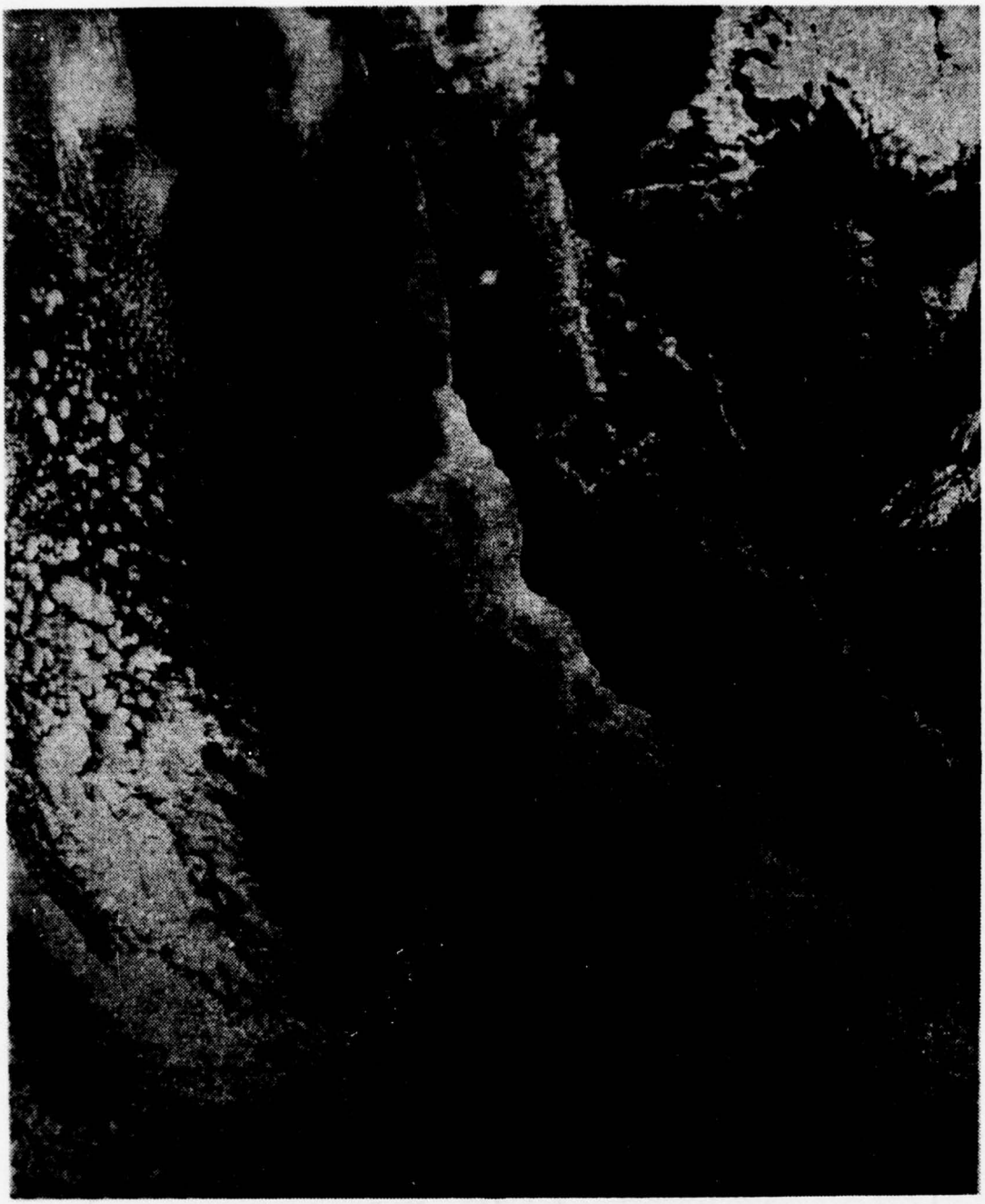

Plate 1. Eastern North Pacific - September 11, 1974, NOAA 3 Satellite, VHRR Infrared Image (Cloudless area) Enhanced for water temperature: (white ~10°C; black ~20°C).

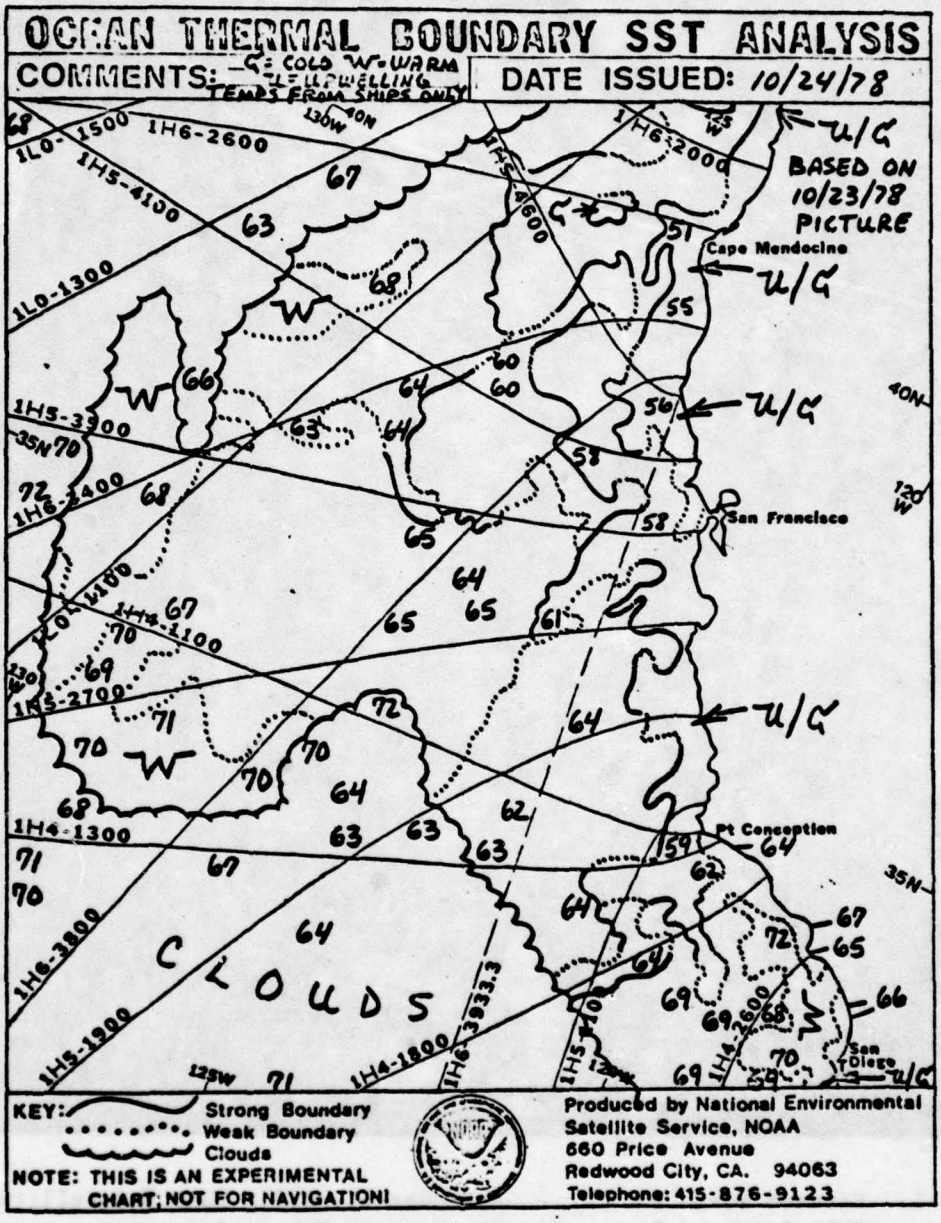

Figure 4a. Thermal front analysis (from Satellite Field Service Station, National Environmental Satellite Service, Redwood City, California).

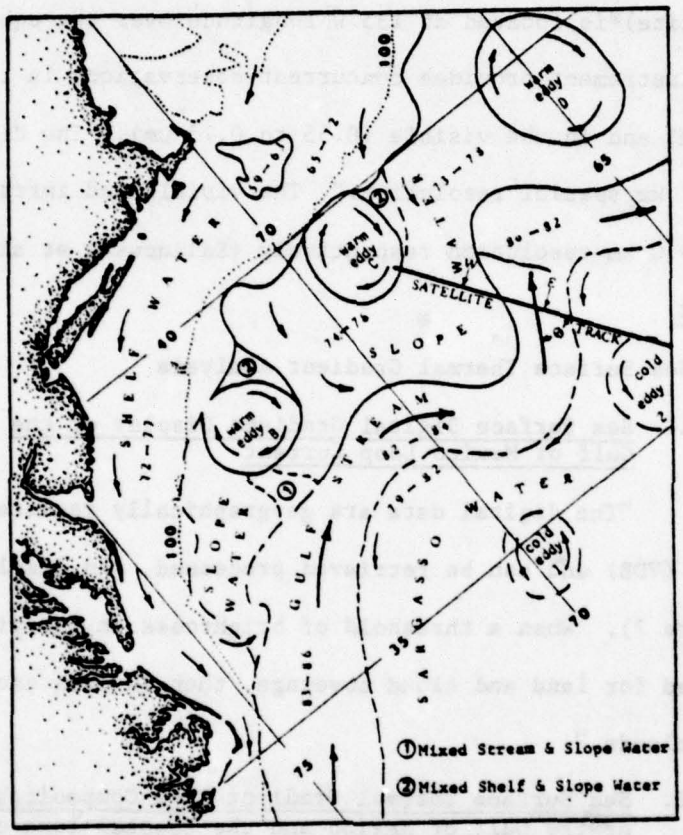

Figure 5. Example of an Experimental Ocean Frontal Analysis (EOFA) chart with subsatellite track for orbit 1795. Water temperatures in °F (from Leitao et al, 1978).

B. GOES-1 AND SMS-2

The following for the most part is a condensation from Miller et al (1977) except where noted. "The two geostationary satellites currently operated by the National Environmental Satellite Service (NESS) carry VISSR instruments. GOES-1 (Geostationary Environmental Satellite) is located at 75°W over the equator and the western satellite SMS-2 (Synchronous Meteorological Satellite) is located at 135°W longitude over the equator (Figure 6). The VISSR instrument provides concurrent observations in the infrared (10.5 to 12.6 μm) and in the visible (0.55 to 0.75 μm). The digital data are at a 7 x 7 km spatial resolution." The visible and infrared channels have a 0.8 and 8.0 km resolution respectively (Kalinowski et al, 1977).

i. VISSR

a. Sea Surface Thermal Gradient Analysis

1. Sea Surface Digital Gradient Display of the Gulf of Mexico Loop Current

"The digital data are geographically registered in the VISSR data base (VDB) and can be retrieved, processed, and displayed in near real time (Figure 7). When a threshold of brightness in the visible is assumed or mapped for land and cloud coverage, then IR data can be screened for effects of clouds."

2. Sea Surface Thermal Gradient Time Composites Display of the Gulf of Mexico and the Coastal Zone of the Eastern United States (Loop Currents and Gulf Stream Wall)

The technique described above can be applied over time to eliminate cloud-edge and partly clouded IR data (see Miller et al, 1977).

3. Experimental Loop Current and Gulf Stream Movie Loops

Another experimental research tool utilizing the multi-look capabilities of the GOES sensors consists of infrared images sequenced in movie form.

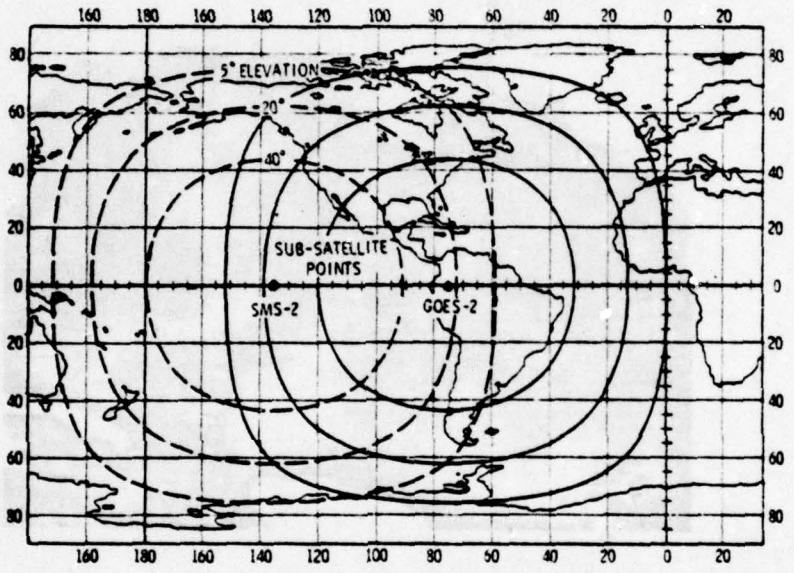

Figure 6. GOES coverage and elevation pattern (from McCall et al, 1977).

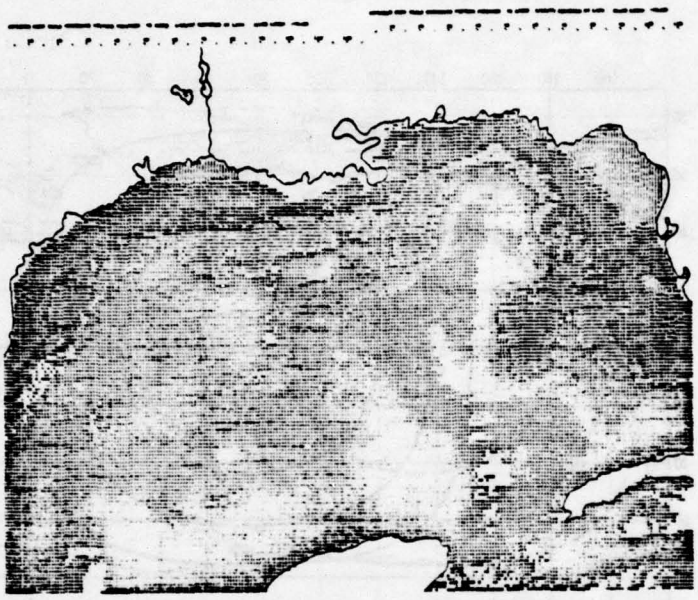

Figure 7. Sea surface digital gradient display of the Gulf of Mexico loop current. Thermal IR digital data were taken from the GOES-1 satellite at 1600 GMT of February 25, 1977. Area displayed is the Gulf of Mexico with States bordering the Gulf, a portion of Western Cuba, and the Northern Yucatan Peninsula outlined by solid black lines. White areas in the display are either land, shallow water areas, or cloud-covered regions at picture time (from Miller et al, 1977).

4. Visible and Thermal Characteristics of Hurricanes

(See Miller et al, 1977.)

C. DMSP

i. WHR, Very High Resolution Infrared (0.3 nm resolution)

a. Ocean Thermal Front Analysis (from Crocker and Spikes, 1977)

1. Pacific Fleet ASW Exercises

"The Director, Naval Oceanography and Meteorology (DNOM) conducts a satellite interpretation program using data from the Defense Meteorological Satellite Program (DMSP) satellite, as read out by antenna vans located at several Fleet Weather Centrals and Fleet Weather Facilities (FWF's). The San Diego FWF has had success in providing frontal and eddy information in support of Pacific Fleet ASW exercises. In addition, some aircraft carriers (USS CONSTELLATION, USS KENNEDY) have satellite readouts that permit the tracking of thermal discontinuities."

2. Mediterranean Fleet ASW Exercises

"Daily readouts provided by the DMSP facility at FWC Rota, Spain are currently used on a routine basis by the Sixth Fleet ASW Force for planning and interpreting ASW operations in the Mediterranean. The percent availability and the causes of inadequate coverage are being noted to assess the overall reliability of the readouts for this area."

D. TIROS-N (Launched in October, 1978)

TIROS-N is operating in "a sunsynchronous, near circular orbit at an altitude of 835 kilometers. The major improvements that TIROS-N will bring the marine community include the Advanced Very High Resolution Radiometer (AVHRR) to replace the SR, the VHRR of the older NOAA polar-orbiting satellite series, and the Data Collection and Platform Location Systems (DCPLS). The DCPLS receives and retransmits telemetered environmental in-situ data

from earth-based platforms to a central process facility" (see Ernst and Sherman, 1977).

i. AVHRR

a. Sea Surface Temperature Fields (from Kalinowski et al, 1977)

"The lauch of TIROS-N initiated a new satellite and data processing system. The increased capabilities of TIROS-N will result in improved present day products and in several new ones, viz.,

1. Movable 2500 Square-Degree Meso-Scale SST Fields having 50 km resolution will be maintained in selected areas. Initially, at least, they are expected to encompass the U. S. 200-mile zone.

2. A Global 500-km Resolution Climatic-Scale Field on a 5° grid will be maintained in support of climatological studies.

3. Full Resolution Digital Data from the AVHRR will be used to prepare weekly hand-drawn isothermal analyses of the Great Lakes and the U. S. Coastal Zone. These will have fishery, shipping and weather forecasting applications."

E. SEASAT-A (Launched June, 1978)

"SEASAT-A is in a non-sunsynchronous, 800 km altitude orbit. The 108 degree orbit inclination with the equator, although high, does not provide for the usual polar coverage. The ground track repeated cycle is 152 days, with an equatorial track grid separation of 18.5 kilometers. The SEASAT-A sensor complement includes the SEASAT-A Scatterometer System (SASS), a Synthetic Aperture Radar (SAR), a Visible and Infrared Radiometer (VIR), a radar altimeter, and a Scanning Multichannel Microwave Radiometer (SMMR)."

i. SMMR

a. Sea Surface Temperature Fields

1. All Weather Sea Surface Temperature

"The winter of 1976-77 illustrated the inability of

present-day satellites to monitor surface parameters through persistent cloud cover. Long periods of cloudiness in the Western Atlantic and Western Pacific allowed the portions of the SST field including the Gulf Stream and the Kuroshio Current off Japan to first become badly outdated" (Kalinowski et al, 1977). The scanning multichannel microwave radiometer (SMMR) will provide SST in all weather with its ability to "see" through clouds to an accuracy of $\pm$ 2°K. Application of SMMR information to delineation of ocean fronts and eddies will be supplemented by information on currents from radar altimeter data (Ernst and Sherman, 1977). Unfortunately, SEASAT-A is no longer functional.

F. NIMBUS-G (Launched September 18, 1978)

"NIMBUS-G has a sun-synchronous orbit. The orbital altitude and inclination is 955 km and 99.28 deg. respectively. The ground trace is repeated every six days with equatorial ground track grid separation at 600 kilometers."

"The NIMBUS-G oceanic sensor compliment consists of the SMMR and a Coastal Zone Color Scanner (CZCS), a new type of multi-spectral space sensor."

i. SMMR

a. Sea Surface Temperature

SEASAT-A and NIMBUS-G will fly identical (passive) SMMR's with all weather capabilities to sense sea surface temperature through clouds to $\pm$ 2°K (Ernst and Sherman, 1978).

ii. The Coastal Zone Color Scanner (CZCS)

"The CZCS is expected to provide useful information on sediment transport processes and biological activity as related to chlorophyll concentrations" (Ernst and Sherman, 1977). These oceanographic characteristics in turn may be useful to detect ocean fronts and eddies when the SST pattern is not present.

V. DETECTION OF OCEAN FRONTS AND EDDIES BY SATELLITE SENSED SEA SURFACE COLOR

A. ANALYSIS OF VARIATIONS IN OCEAN COLOR

Ocean color, or the upwelling radiation of sunlight reflected or back-scattered by seawater in the visible spectrum is influenced by absorbing and scattering material which is dissolved or suspended (Deschamp et al, 1977; Morel and Prieur, 1977). At one extreme is water with high concentrations of chlorophyll-bearing phytoplankton (Figures 8a and d) which appears very green in color. At the other extreme is water which has high concentrations of suspended inorganic particles (Figures 8c and f). This water has a milky green appearance. In between is the deep blue color characteristic of very pure seawater which has very little if any dissolved or suspended, organic or inorganic material present (Figures 8b and c). The satellite sensors operate on the principle that by selecting the proper spectral channels (see Table 1 from Hovis and Leung, 1977) small changes in the spectral radiance between two or more wavelength regions can be used to indicate the presence of phytoplankton (Kim et al, 1977). For the purpose of detection of ocean fronts and eddies it should be remembered that nutrient enriching mixing processes which are associated with the formation of ocean fronts and eddies may lead to relatively dense populations of phytoplankton.

"The qualitative and quantitative analysis of dissolved and particulate matter by remote sensing of the color of the ocean presents two problems" (Morel and Prieur, 1977). The first problem is getting significant oceanographic information which represents only 20% or less of the total signal received in a remote optical sensor (Hovis and Leung, 1977). The second problem is interpretation of the reflected signal in relationship to the

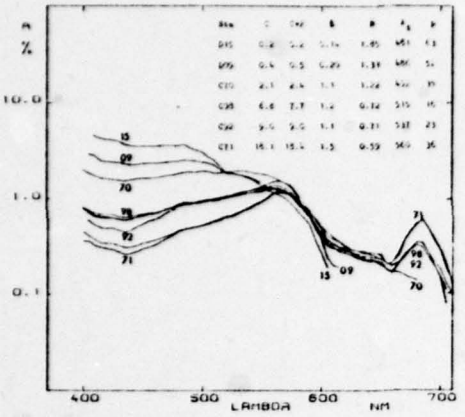

8a. Experimental R(λ) curves for different stations listed in inset: D stations--Discoverer cruise; C stations--CINECA 5-Charcot cruise. C and C+P--chlorophyll a + pheophytin a concentration in mg m^{-3}; b-scattering coefficient at 550 nm (from Morel and Prieur, 1977)

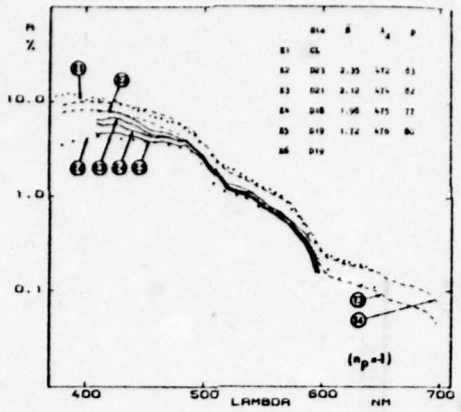

8b. Theoretical dashed curves T3 and T4. Experimental dotted curve E1 concerns Crater Lake (Oregon); E2-E6 concern Sargasso Sea and these experiments were carried out during Discoverer cruise (stations D23, D21, D18, and D19)(from Morel and Prieur, 1977)

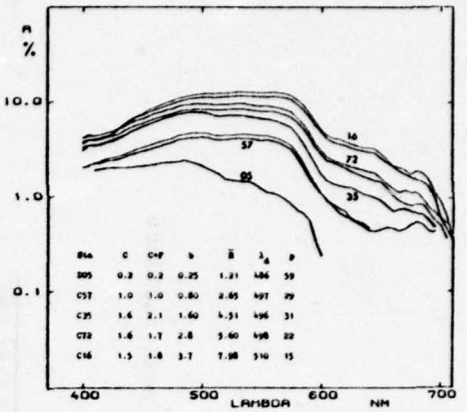

8c. Experimental R(λ) curves. Symbols same as for Fig. 8a (from Morel and Prieur, 1977)

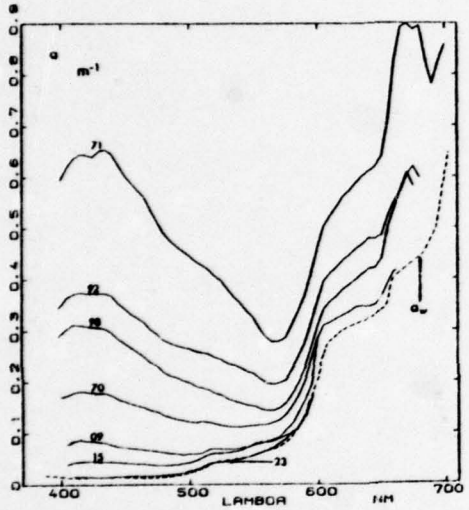

8d. Spectral values of absorption coefficient expressed in m^{-1}, for same stations as in Fig. 8a. In addition, values for station Discoverer 23 (Sargasso Sea) and for pure water (labeled a_w) are plotted (from Morel and Prieur, 1977)

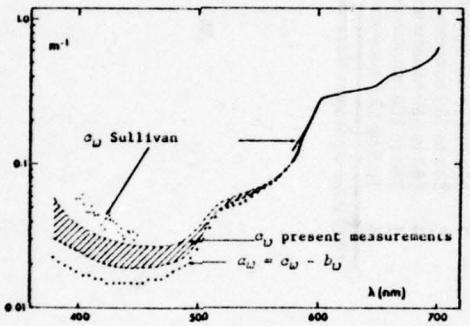

8e. Attenuation, $c_u(\lambda)$, and absorption coefficient, $a_u(\lambda)$, expressed in m^{-1}, for pure water (from Morel and Prieur, 1977)

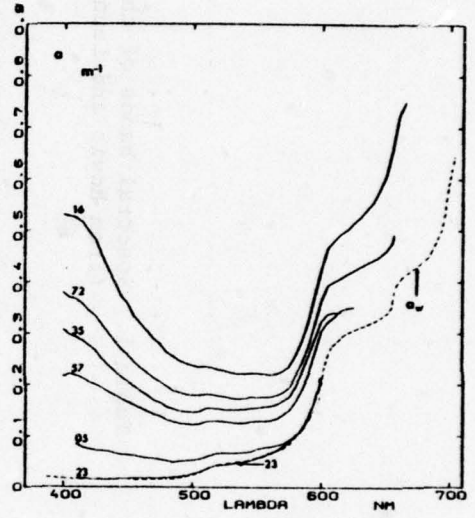

8f. Spectral values of absorption coefficient, expressed in m^{-1}, for same stations as in Fig. 8c (from Morel and Prieur, 1977)

Table 1. Spectral bands of the CZCS and peak radiance (from Hovis and Leung, 1977).

Channel	Spectral Range	Peak	Radiance mw/cm² ster.		μm
1	433 to 453 nanometers	11.46	7.64	6.21	2.88
2	510 to 530 nanometers	7.64	6.20	5.10	3.50
3	540 to 560 nonometers	6.21	5.10	4.14	2.86
4	660 to 680 nanometers	2.88	2.32	1.91	1.34
5	700 to 800 nanometers	23.9			
6	10.5 to 12.5 micrometers	*			

*Will sense equivalent blackbody temperature from 270 to 320 K.

water's optical properties which in turn are subordinate to the content of dissolved and particulate matter. The second problem will be discussed first. The following is a condensation of the paper "Analysis of Variations in Ocean Color" by Morel and Prieur (1977).

i. Reflectance

The reflectance can be calculated for seawaters which are different with respect to turbidity and pigment content. These results can be used in the inverse process to infer the turbidity or pigment content from remotely sensed reflectance measurements. Reflectance $R(\lambda)$ is expressed as a ratio of the upwelled irradiance just below the surface, $E_u(\lambda)$, to downwelling irradiance just above the surface, $E_d(\lambda)$, where λ is the wavelength, viz.,

$$R(\lambda) = E_u(\lambda)/E_d(\lambda) \tag{1}$$

The reflectance ratio is dependent on the absorption coefficient (a) and the backscattering coefficient (b') and can be calculated by the expression

$$R = 0.33\ (b'/a) \tag{2}$$

ii. Backscattering Coefficient

The backscattering coefficient is expressed as the sum

$$b' = b_w' + b_p' \tag{3}$$

where b_w' and b_p' stand for molecular and particle scattering respectively. For optically pure water (no particles)

$$b_w'/b' \equiv 1 \tag{4}$$

i.e., backscattering is all molecular. For very turbid waters

$$b_w'/b' \to 0 \tag{5}$$

i.e., backscattering is mostly particulate. The wavelength dependence of b' must always be taken into consideration. While molecular scattering is a minor and often negligible factor when the total scattering is considered, it plays an important role in backscattering. Backscattering and the proportion which is molecular may vary greatly with wavelength. The wavelength dependence of molecular scattering can be expressed in terms of a power law, the most suitable being

$$b_w' \sim \lambda^{-4.3} \tag{6}$$

A similar law can be used for particle scattering. In most cases

$$b_p' \sim \lambda^{-1} \tag{7}$$

describes the distributions.

iii. Absorption Coefficient (for pure water)

The total scattering coefficient, b, is well known for pure seawater (meaning without a trace of dissolved organic substances or particulates) or pure water. If the attenuation coefficient c_w is known, the absorption coefficient a_w can be obtained by difference viz.

$$a_w = c_w - b_w \tag{8}$$

In Figure 8e note the minimum attenuation and minimum absorption between 430 and 470 nm, the increase of both absorption and attenuation between 500 and 520 nm and that at ca 600 nm, $c_w \simeq a_w$ (i.e., attenuation is about the same as absorption because there is very little molecular scattering).

The reflectance ratio, $R(\lambda)$, can be calculated using equation 2, the absorption coefficients for pure water (Table 2) and b' which is calculated from $b_w(\lambda)$ values pertaining to optically pure seawater which are about 30% higher than for pure water. Figure 8b shows the theoretical dashed curve T3 and T4 which are the spectral reflectance ratios computed for two cases. Since the absorption is that for pure water, it shows that all $R(\lambda)$ values increase with backscattering. It also shows the variation of R over the spectral range as R is changed by molecular and particle scattering.

iv. Blue Waters

In clear blue ocean water such as the Sargasso Sea the blue reflectance (curves E2-E6 Figure 8b) is due to the balance of molecular backscattering to water absorption in chemically pure water. A small amount of phytoplankton and "yellow substance" probably explains the increase in absorption and consequently the decrease of R in the blue-violet part of the spectrum at several stations in the Sargasso Sea. The spectral reflectance curve, E1, in Crater Lake, while pure relative to absorption, indicates particle backscattering twice that for the Sargasso Sea. In any case the theory for spectral R values and for color is satisfactory for these very clear waters. But, what about green waters?

v. Various Green Waters

In productive and turbid waters the presence of dissolved and suspended matter increases both absorption and scattering. When backscattering increases, R increases as predicted by equation one and more or less uniformly throughout the spectrum. On the other hand, R decreases as absorption increases, but especially in the spectral bands which correspond to the absorption of various substances present (compare Figures 8a with 8d and 8c with 8f).

Table 2. Attenuation (c_w), scattering (b_w), and absorption (a_w) coefficients for optically (and chemically) pure water (from Morel and Prieur, 1977).

λ (nm)	c_w (m^{-1})	b_w (m^{-1})	a_w (m^{-1})	λ (nm)	c_w (m^{-1})	b_w (m^{-1})	a_w (m^{-1})	λ (nm)	c_w (m^{-1})	a_w (m^{-1})	b_w (m^{-1})
380	0.050	0.0073	0.023	490	0.022	0.0024	0.020	600	0.245	0.00101	
390	0.027	0.0066	0.020	500	0.028	0.0022	0.026	610	0.290	0.00064	
400	0.024	0.0058	0.018	510	0.038	0.0020	0.036	620	0.310	0.00068	
410	0.022	0.0052	0.017	520	0.050	0.0018	0.048	630	0.320	0.00082	
420	0.021	0.0047	0.016	530	0.053	0.0017	0.051	640	0.330	0.00074	
430	0.019	0.0043	0.015	540	0.058	0.0016	0.056	650	0.350	0.00077	
440	0.019	0.0039	0.015	550	0.066	0.0015	0.064	660	0.410	0.00067	
450	0.018	0.0035	0.015	560	0.072	0.0013	0.071	670	0.430	0.00063	
460	0.019	0.0032	0.016	570	0.081	0.0013	0.080	680	0.450	0.00059	
470	0.019	0.0029	0.016	580	0.109	0.0012	0.108	690	0.500	0.00055	
480	0.021	0.0027	0.018	590	0.158	0.0011	0.157	700	0.650	0.00050	

vi. Blue-Green to Dark Blue-Brown Waters

Absorbing materials are present in high concentrations when chlorophyll concentration is high. R values in the blue-violet region decrease and a minimum is formed at ca. 440 nm (Figure 8a) which corresponds to the maximum absorption of chlorophyll (Figure 8d). As the absorption due to pigments is at a minimum between 565-570 nm and absorption due to water itself just begins to rapidly decrease (Figure 8d), R values form a maximum at ca. 560 nm (Figure 8a). There is a slight irregularity at ca. 480 nm which may be due to absorption by carotenoid pigments. The second maximum of absorption by chlorophyll a creates an R minimum near 665 nm (Figure 8a) but it is only slightly marked because the increase due to absorption by chlorophyll is small relative to absorption due to water itself (Figure 8d). A second R maximum appears at 685 nm. This maximum may be due to a combination of enhanced backscattering by pigment particles in the vicinity of their absorption bands plus the 685 nm fluorescence peak from chlorophyll a. This fluorescence radiation is in upwelling radiance but absent in downwelling, the so called Fraunhofer line or that part of the spectrum of solar radiation which is absorbed in the sun's atmosphere. Therefore, R would increase as defined ($R(\lambda) = E_u(\lambda)/E_d(\lambda)$. Where the reflectance curves are the same, even for different concentrations of chlorophyll as in the 560-640 nm spectral band (Figure 8a) the increased absorption due to increased chlorophyll is about compensated for by increased backscattering. The mean reflectance ratio, R, which is obtained by integrating $R(\lambda)$ between 380 and 700 nm, becomes very low when the phytoplankton concentration increases (see table inset in Figure 8a) and the color of the water is from blue-green to dark green-brown.

vii. Blue-Green or Green with a Bright Milky Appearance

Scattering materials are present in high concentrations when

waters are higher in inorganic particles than in phytoplankton and the reflectance spectrum is different (Figure 8c). R values are higher throughout the spectrum and the curve is a different shape. There is no minimum at 440 nm due to absorption. The R maximum, due to low absorption by pigment or water itself, is still located at ca 560 nm, but the curves are convex between 400 and 560 nm. The increase in backscattering, R, with increase of turbidity is not compensated by a proportional increase in absorption. In fact R becomes higher as turbidity increases which is just the opposite of the high phytoplankton low inorganic material case. These waters are blue-green or green with a bright milky appearance.

A number of attempts have been made to determine if $R(\lambda)$ values (after correction for atmospheric deterioration and illumination changes) can provide an estimate of pigment concentration, principally chlorophyll, and suspended non-chlorophyll materials.

B. RADIATIVE TRANSFER AND THE ATMOSPHERIC STATE

Backscatter of sunlight by the atmosphere increases the total signal as a function of altitude (Figure 9) making the oceanographic signal more and more difficult to detect (Clarke et al, 1970 and Hovis and Leung, 1977). The backscatter consists of reasonably predictable Rayleigh scattering and unpredictable Mie scattering (Hovis and Leung, 1977). The former is scattering of radiation from density fluctuations rather than from molecules. It explains the blue color of the sky. The latter is defined as scattering of electromagnetic radiation by homogeneous dielectric spheres (see Wezernak et al, 1976). It constitutes the majority of the signal seen by a high altitude sensor (Hovis and Leung, 1977).

The atmosphere will also scatter and absorb radiation reflected from the sea and thereby alter the intrinsic radiation characteristics (Wezernak

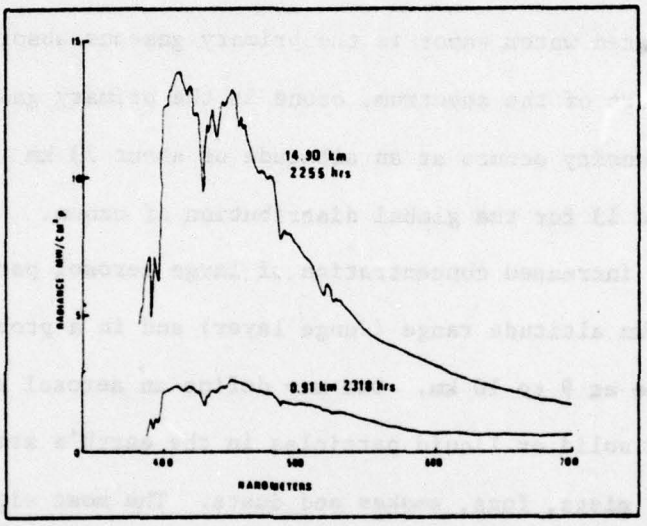

Figure 9. Upwelling radiance over Catalina Channel at high and low altitude (from Hovis and Leung, 1977).

et al, 1976). The major concerns are the scattering and absorbing properties of gases and particulates that exist in the atmosphere (Wezernak et al, 1976). The major permanent gases, oxygen, nitrogen and argon, absorb very little in the visible and near infrared. Only variable components such as water vapor, carbon dioxide, sulfur dioxide, ozone, nitrogen compounds, methane and other trace gases absorb such radiation to any extent. Spectral regions in which absorption is at a minimum can be selected since the gaseous absorption regimes of atmospheric gases are well known (see Figure 10). In the near infrared water vapor is the primary gaseous absorber. Throughout the visible part of the spectrum, ozone is the primary gaseous absorber. The maximum density occurs at an altitude of about 23 km (Figure 11). See Figures 12 and 13 for the global distribution of ozone.

A zone of increased concentration of large aerosol particles exists in the 17 to 23 km altitude range (Junge layer) and in a probable layer under the tropopause at 9 to 10 km. One may define an aerosol as a semi-permanent suspension of solid or liquid particles in the earth's atmosphere, e.g., haze, clouds, mists, fogs, smokes and dusts. The most significant aspect of aerosol particles in the atmosphere is their high degree of variability in composition, size, distribution and especially in number density. All the models in the current literature deal with a highly approximate average condition from which large deviations can occur in real situations.

Wezernak et al (1976) have used a radiative-transfer model in analyzing multi-spectral remote sensing data. The multiple scattered radiation field within the earth's atmosphere can be calculated. Atmospheric corrections have been applied to data of surface waters to reduc the data to surface level. Reflectance data were converted to radiance data at satellite altitude for a specific set of conditions.

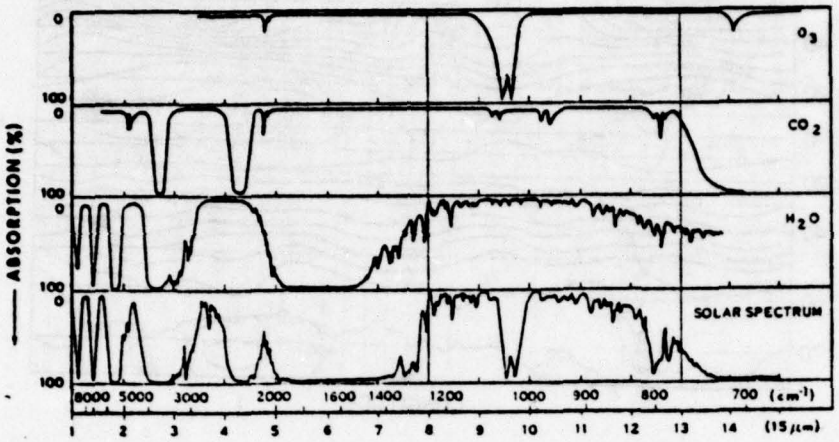

Figure 10. Comparison of near infrared solar spectrum with laboratory spectra of various atmospheric gases (from Fett and Mitchell, 1977).

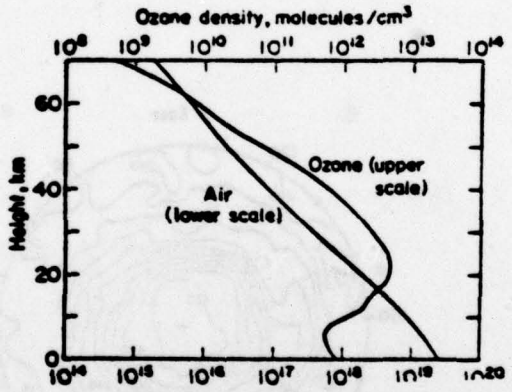

Figure 11. Midlatitude vertical distributions of air density (lower scale) and ozone density (upper scale) in the troposphere, stratosphere, and lower mesosphere. The air density distribution is from the U.S. Standard Atmosphere (1962), the ozone density distribution is from Krueger and Minzner (1973). Note that the air density scale is 10^6 times the ozone density scale, so that the ratio of the two curves at any height subjectively gives the ozone mixing ratio in ppm (National Research Council, 1975) (from Holland, 1978).

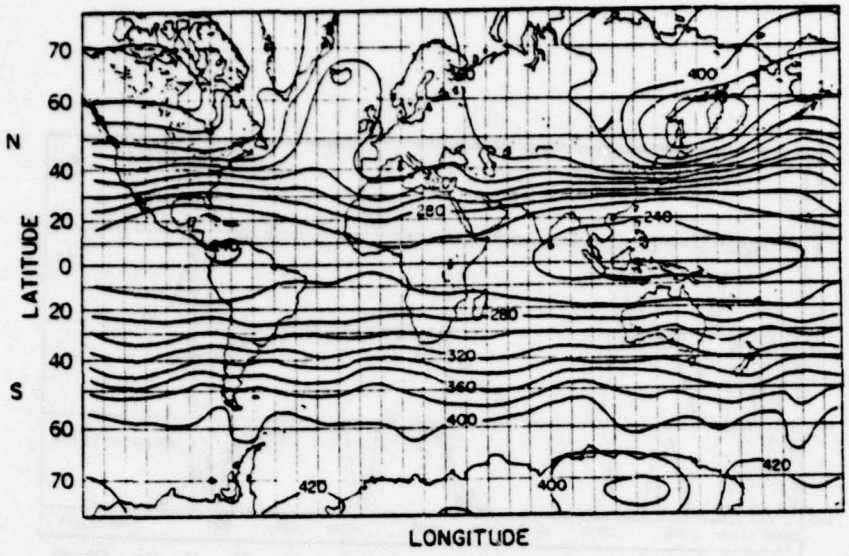

Figure 12. Global distribution of total ozone (Dobson units) derived from NIMBUS 4 IRIS measurements for December 1970 (from Prabhakara and Rodgers, 1976).

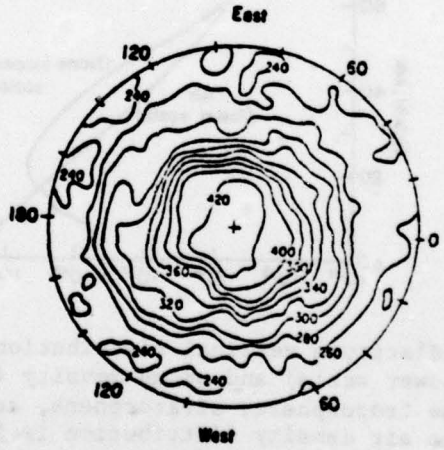

Figure 13. Total ozone in the northern hemisphere as measured from NIMBUS IV satellite, May 1969. Contour lines are in units of milliatmosphere-centimeters STP (Dobson units) (National Research Council, 1975). Reproduced with the permission of the National Academy of Sciences (from Holland, 1978).

C. REMOTE SENSING OF OCEAN COLOR

Notwithstanding atmospheric effects, color of the sea surface has been remotely sensed with virtually the entire atmosphere interposed and interpreted in terms of chlorophyll content and suspended matter. In a U-2 study (Hovis and Leung, 1977), upwelling and radiance was measured in ten spectral bands at an altitude of 19.8 km (Table 3). The radiance in four of these bands (471, 547, 583 and 666 nm, Figure 14) was at first compared with chlorophyll concentrations along scan lines which coincided with the ship tracks along which the pigment measurements were made.

i. Color Ratios

Reflectance ratios for various combinations of the four spectral bands were correlated with chlorophyll concentration. The 547 and 662 nm bands worked best in the formula

$$\frac{R_{662}}{R_{547}} = a + b \log_e C \qquad (9)$$

where R_{662} = radiance (unenhanced) at 662 nm

R_{547} = radiance (unenhanced) at 547 nm

$a = 0.309$

$b = 0.0166$

C = chlorophyll mg/m^3

While the correlation between calculated and measured chlorophyll (Figure 15) is not perfect, the same algorithm can be applied to an entire scene to produce an "enhanced color image" (see Hovis and Leung, 1977).

ii. Accounting for Atmospheric Effect in Chlorophyll and Sediment Signatures

There is no provision in these color ratio-algorithms for variations in atmospheric backscattering intensity and spectral distribution

Table 3. Parameters of the U-2 ocean color scanner (from Hovis and Leung, 1977).

Channel	Center Wavelength (nm)	Bandwidth (nm)	Radiance (Gain x 1) mw/cm² μ
1	433	22.5	40.1
2	471	21.5	26.0
3	509	27.5	23.6
4	547	24.5	14.7
5	583	25.0	11.8
6	620	26.0	10.0
7	662	22.0	7.55
8	698	20.5	5.0
9	733	22.5	11.9
10	772	23.0	3.47

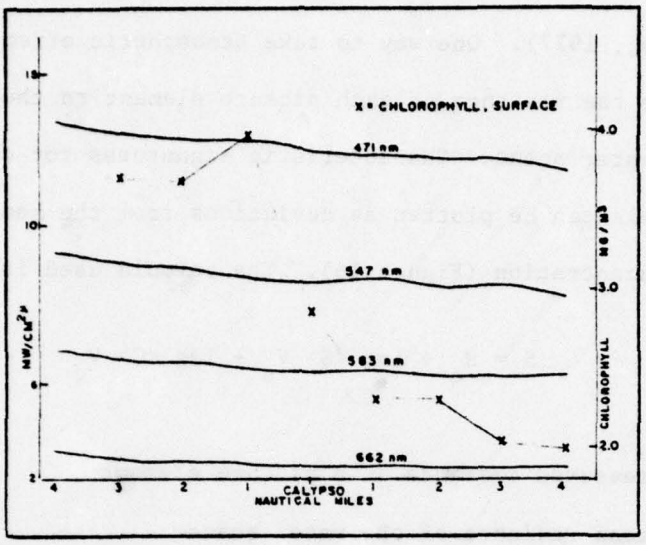

Figure 14. Upwelling radiance along one scan line in four spectral bands vs chlorophyll concentration (from Hovis and Leung, 1977).

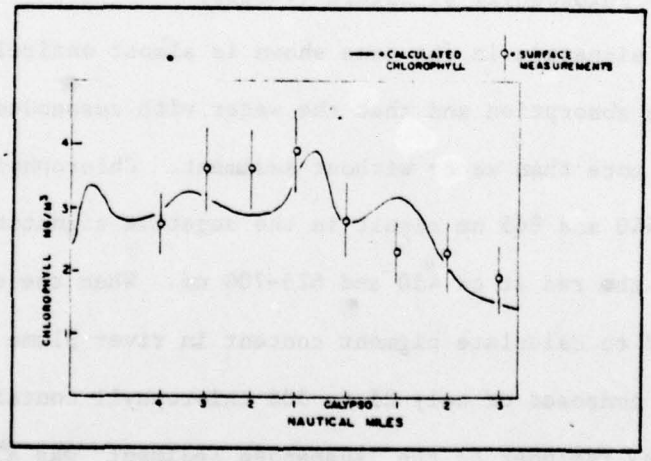

Figure 15. Calculated vs measured chlorophyll concentration, Gulf of Mexico (from Hovis and Leung, 1977).

caused by variations in such parameters as cloud cover and aerosol content. At this time there is no way to measure these changes from a satellite (Hovis and Leung, 1977). One way to take atmospheric effect into account is to reference the radiance of each picture element to the mean radiance of the entire water scene. Characteristic signatures for chlorophyll and suspend materials can be plotted as deviations from the mean radiance as a function of concentration (Figure 16). The formula used is

$$S = S_o + \log \langle S \rangle V_s + \log \langle C \rangle V_c \qquad (10)$$

where S = measured radiance at a picture element

S_o = mean radiance of the water scene

$\langle S \rangle$ = sediment concentration

$\langle C \rangle$ = chlorophyll concentration

V_s = sediment signature (vector)

V_c = chlorophyll signature (vector)

The sediment signature in the case shown is almost entirely positive indicating little absorption and that the water with suspended "sediment" backscatters more than water without sediment. Chlorophyll's two absorption bands at ca 440 and 665 nm result in the negative signature components in the blue and the red at ca 450 and 625-700 nm. When the chlorophyll signature was used to calculate pigment content in river plume samples containing sediment composed of only 25 to 30% chlorophyll containing organisms by weight (the reminder of the "suspended sediment" was almost entirely the residue of organisms) there was considerable variance in the correlation with measured chlorophyll (Figure 17). The backscattering from the sediment apparently overwhelms the effect of chlorophyll absorption. On the other hand, when sediment concentrations were computed from the remotely sensed radiance data there was good agreement with measured concentrations (Figure 18).

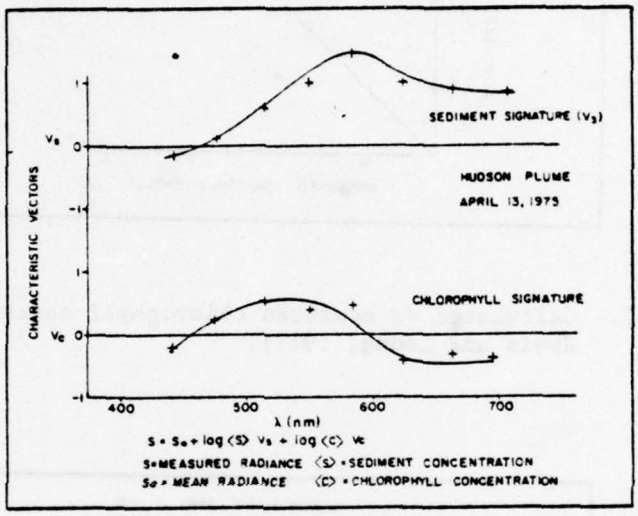

Figure 16. Characteristic signatures, sediment and chlorophyll, New York Bight, April 1975 (from Hovis and Leung, 1977).

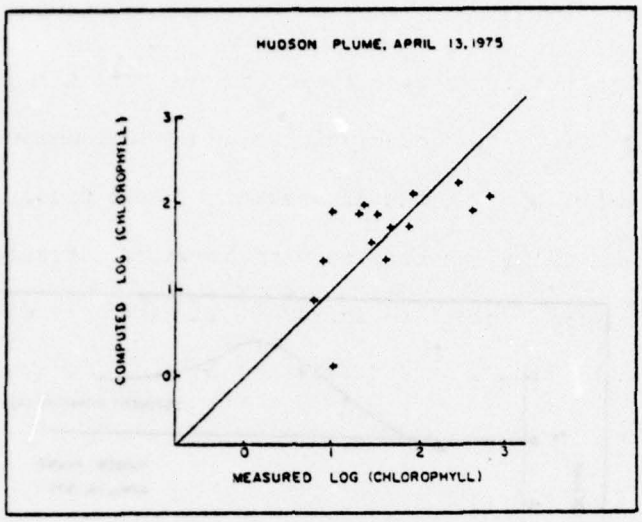

Figure 17. Calculated vs measured chlorophyll concentration (from Hovis and Leung, 1977).

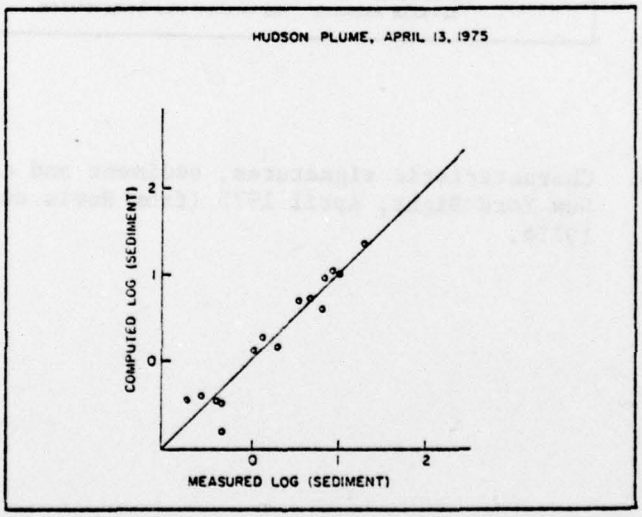

Figure 18. Calculated vs measured sediment concentration (from Hovis and Leung, 1977).

VI. CONCLUSION

Improvements in satellite technology have allowed the description of fronts at the surface of the ocean which can have a considerable impact on the performance of Naval acoustic systems. These fronts are detected by thermal discontinuities associated with boundary currents, eddies and upwelling. At present, satellite infrared data which is used in the description of thermal fronts is intermittent in time and space, because of cloud cover, seasonal variability of sea surface temperature gradients and the quality of the electronic signal. The coverage and quality of thermal data is improving with the introduction of new satellites with sensors which can see through clouds. Now with the launching of NIMBUS G there is considerable promise that color characteristics can be used to detect ocean fronts and eddies when the sea surface temperature pattern is not present.

LIST OF REFERENCES

1. Clarke, G. L., G. C. Ewing and C. J. Lorenzen (1970) Spectra of backscattered light from the sea obtained from aircraft as a measure of chlorophyll concentration. Science, 167, 1119-1121.

2. (U) Crocker, K. T., and C. H. Spikes (1977) Effects of ocean fronts and eddies on ASW in the North Atlantic. Rept. No. CLF/NSAP 4-76. Naval Underwater Systems Center, Newport, Rhode Island 02840, 1-38.

3. Deschamps, P. Y., P. Lecomte and M. Viollier (1977) Remote sensing of ocean color and detection of chlorophyll content. In: Proceedings of the Eleventh International Symposium on Remote Sensing of Environment, Environmental Research Institute of Michigan, Ann Arbor, Michigan, Volume II, 1021-1034.

4. Ernst, J. A. and J. W. Sherman (1977) A space focus for oceanography. Conference on Satellite Applications to Marine Technology, New Orleans, Louisiana. Copyright American Institute of Aeronautics and Astronautics, Inc., 34-38.

5. Fett, R. W. and W. F. Mitchell (1977) Navy tactical applications guide. Volume I, Techniques and applications of image analysis. Defense Meteorological Satellite Program, Naval Environmental Prediction Research Facility, Monterey, California 93940, Applications report 77-03.

6. Holland, H. D. (1978) The chemistry of the atmosphere and oceans. A Wiley-Interscience Publication, John Wiley and Sons, New York, 351 pp.

7. Hovis, W. A. and K. C. Leung (1977) Remote sensing of ocean color. Optical Engineering, 16, 158-166.

8. Kalinowski, J. K., T. L. Signore, W. G. Pichel, C. C. Walton, R. L. Brower, S. R. Brown and K. G. Bennekamper (1977) Present and Future operational NOAA satellite oceanographic products: An introduction. In: Proceedings of the Eleventh International Symposium on Remote Sensing of Environment, Environmental Research Institute of Michigan, Ann Arbor, Michigan, Volume I, 625-633.

9. Kim, Hongsuk H., L. R. Blaine, R. S. Fraser, N. E. Huang, and H. van der Piepen (1976) A proposal for an ocean color experiment for orbital flight test 2. Office of Planning and Program Integration National Aeronautics and Space Administration, Washington, D.C., 18 pp.

10. Legeckis, R. (1978) A survey of worldwide sea surface temperature fronts detected by environmental satellites. Journal of Geophysical Research, 83:C9, 4501-4522.

11. Leitao, C. D., N. E. Huang and C. G. Parra (1978) Remote sensing of Gulf Stream using GEOS-3 radar altimeter. NASA Technical Paper 1209, National Aeronautics and Space Administration, Wallops Flight Center, Wallops Island, Virginia 23337, 31 pp.

12. McCall, J. G., E. G. Kerut and G. Haas (1977) Satellite application to data buoy requirements. Conference on Satellite Applications to Marine Technology, New Orleans, Louisiana. Copyright, American Institute of Aeronautics and Astronautics, Inc., 135-144.

13. Miller, D. B., M. P. Waters, III, J. D. Tarpley, R. N. Green and D. C. Dismachek (1977) Potential applications of digital, visible and infrared data from geostationary environmental satellites. IN: Proceedings of the Eleventh International Synposium on Remote Sensing of Environment, Environmental Research Institute of Michigan, Ann Arbor, Michigan, Volume I, 1849-1858.

14. Morel, A. and L. Prieur (1977) Analysis of variations in ocean color. Limnology and Oceanography, 22(4), 709-722.

15. Nagler, R. G. (1977) Surveying the earth's environment from space: spectral, areal, temporal coverage trends. Conference on Satellite Applications to Marine Technology, New Orleans, Louisiana. Copyright, American Institute of Aeronautics and Astronautics, Inc., 157-166.

16. Prabhakara, C. and E. B. Rodgers (1976) Study of the lower stratospheric thermal structure and total ozone from Nimbus-4 IRIS. Goddard Space Flight Center, Greenbelt, Maryland 20771, NASA TN D-8134, 35 pp.

17. Sherman, J. W., III (1977) Current and future satellites for oceanic monitoring. In: Proceedings of the Eleventh International Symposium on Remote Sensing of Environment, Environmental Research Institute of Michigan, Ann Arbor, Michigan, Volume I, 288-299.

18. U. S. Department of Commerce (1978) Sea surface temperature °F, September 1-14. National Oceanic and Atmospheric Administration, National Marine Fisheries Service, Southwest Fisheries Center, P. O. Box 271, La Jolla, California 92037.

19. Wezernak, C. T., R. E. Turner and D. R. Lyzenga (1976) Spectral reflectance and radiance characteristics of water pollutants. Environmental Research Institute of Michigan, Ann Arbor, Michigan 48107, NASA CR-2665, 218 pp.

INITIAL DISTRIBUTION LIST

		No. Copies
1.	Defense Documentation Center Cameron Station Alexandria, Virginia 22314	2
2.	Library, Code 0142 Naval Postgraduate School Monterey, California 93940	2
3.	Commanding Officer Naval Ocean Systems Center - Attn: Code 531 San Diego, California 92152	2
4.	Dr. Dale Leipper (Chairman) Code 68Lr Department of Oceanography Naval Postgraduate School Monterey, California 93940	1
5.	Dr. Eugene D. Traganza, Code 68Tg Department of Oceanography Naval Postgraduate School Monterey, California 93940	35
6.	Dean of Research, Code 012 Naval Postgraduate School Monterey, California 93940	1
7.	Dr. Warren W. Denner, Code 68Dw Department of Oceanography Naval Postgraduate School Monterey, California 93940	2